



## Original Articles

Dihydroartemisinin inhibits the development of colorectal cancer by GSK-3 $\beta$ /TCF7/MMP9 pathway and synergies with capecitabine

Xiaoshuo Dai <sup>a,1</sup>, Wei Chen <sup>a,1</sup>, Yan Qiao <sup>a,b,c</sup>, Xinhuan Chen <sup>a,b,c</sup>, Yihuan Chen <sup>a</sup>, Kai Zhang <sup>a</sup>, Qiushuang Zhang <sup>a</sup>, Xiaoxuan Duan <sup>a</sup>, Xiang Li <sup>a,b,c</sup>, Jimin Zhao <sup>a,b,c</sup>, Fang Tian <sup>a,b,c</sup>, Kangdong Liu <sup>a,b,c</sup>, Ziming Dong <sup>a,b,c</sup>, Jing Lu <sup>a,b,c,\*</sup>

<sup>a</sup> Department of Pathophysiology, School of Basic Medical Sciences, Zhengzhou University, Zhengzhou, Henan Province, 450001, PR China

<sup>b</sup> Collaborative Innovation Center of Henan Province for Cancer Chemoprevention, Zhengzhou University, Zhengzhou, Henan Province, 450001, PR China

<sup>c</sup> State Key Laboratory of Esophageal Cancer Prevention & Treatment, Zhengzhou University, Zhengzhou, Henan Province, 450052, PR China

## ARTICLE INFO

## Keywords:

Dihydroartemisinin  
Colorectal cancer  
Capecitabine  
GSK-3 $\beta$

## ABSTRACT

Patients with colorectal cancer (CRC) suffer from poor prognosis and lack effective drugs. Dihydroartemisinin (DHA) has anti-cancer potential but the mechanism remains unclear. We elucidated the effects and mechanism of DHA on CRC development with the aim of providing an effective, low-toxicity drug and a novel strategy for CRC. Herein, proliferation assay, transwell assay, tube formation assay, metastasis models, PDX model and AOM/DSS model were used to reveal the effects of DHA on CRC. The key pathway and target were identified by RNA-seq, ChIP, molecular docking, pull down and dual-luciferase reporter assays. As a result, DHA showed a strong inhibitory effect on the growth, metastasis and angiogenesis of CRC with no obvious toxicity, and the inhibitory effect was similar to that of the clinical drug Capecitabine (Cap). Indeed, DHA directly targeted GSK-3 $\beta$  to inhibit CRC development through the GSK-3 $\beta$ /TCF7/MMP9 pathway. Meaningfully, DHA in combination with Cap enhanced the anti-cancer effect, and alleviated Cap-induced diarrhoea, immunosuppression and inflammation. In conclusion, DHA has the potential to be an effective and low-toxicity drug for the treatment of CRC. Furthermore, DHA in combination with Cap could be a novel therapeutic strategy for CRC with improved efficacy and reduced side effects.

## 1. Introduction

Colorectal cancer (CRC) is one of the most dangerous malignancies of the digestive system with the third highest incidence and the second highest mortality rate in the world [1]. It is predicted to increase to 2.2 million new cases and 1.1 million new deaths worldwide by 2030 [2]. Nevertheless, more than 80 % of patients are diagnosed at an advanced stage with metastases, and the 5-year survival rate is only 15.1 % [3]. Furthermore, existing chemotherapeutic drugs such as 5-Fu, capecitabine (Cap), oxaliplatin and irinotecan are often associated with severe side effects and drug resistance, which reduces their therapeutic efficacy [4]. Cap is the first-line clinical agent for the treatment of CRC, especially metastatic CRC [5]. However, Cap shows a high incidence of adverse reactions, with nausea (82.7 %) and diarrhoea (62.5 %) being

the most common, followed by vomiting (54.8 %) and fatigue (54.8 %) [4]. Meanwhile, some combination treatments have shown various safety concerns despite improved therapeutic outcomes [6]. Therefore, patients still face a number of problems, such as high morbidity, poor prognosis and dose limitation due to toxicity, so the search for new drugs to inhibit CRC development can be considered as an effective strategy to address these problems.

Artemisinin is derived from the annual Compositae family member *Artemisia annua* L., which has been used as a traditional Chinese medicine for more than 2000 years. Dihydroartemisinin (DHA), the active metabolite of Artemisinin and its derivatives (ARTs), has been demonstrated as an effective and fast-acting antimalarial drug [7]. Recently, the "new use of old drugs" has attracted more attention due to the known pharmacokinetic and safety information. DHA has received increasing

\* Corresponding author. Department of Pathophysiology, School of Basic Medical Sciences, Zhengzhou University, No.100 Science Road, Zhengzhou, Henan Province, 450001, PR China.

E-mail address: [lujing@zzu.edu.cn](mailto:lujing@zzu.edu.cn) (J. Lu).

<sup>1</sup> These authors contributed equally to this work.

attention for its anticancer functions, such as inhibition of tumor growth, induction of apoptosis, autophagy and endoplasmic reticulum stress [8]. Especially, reports on DHA in CRC mainly focus on the proliferation and cell cycle, but the mechanism and target have not been elucidated [9,10]. Considering the acute clinical problems such as easy metastasis, poor prognosis and toxicity of existing drugs, we aim to systematically explore the pharmacological functions of DHA in CRC, thus providing a basis for the clinical treatment of DHA in CRC.

Aberrant Wnt signaling is considered to be an oncogenic driving pathway of most colorectal malignancies [11]. GSK-3 $\beta$  is an evolutionarily conserved serine/threonine kinase whose activity plays a key role in the Wnt/ $\beta$ -catenin pathway [12]. In the absence of Wnt, GSK-3 $\beta$  phosphorylates  $\beta$ -catenin at Ser33/37/Thr47. Thus,  $\beta$ -catenin is ubiquitinated and destroyed by the proteasome complex. In the presence of Wnt ligand, the Wnt protein ligand binds to the receptor complex and inactivates GSK-3 $\beta$ , thereby inhibiting  $\beta$ -catenin degradation by recruiting Dvl and disrupting the formation of the Axin/GSK-3 $\beta$ /APC complex. The accumulated cytoplasmic  $\beta$ -catenin is then translocated to the nucleus and combines with TCF/LEF to initiate the transcription of targeted genes. GSK-3 $\beta$  is regulated by phosphorylation at Ser9 (inhibition) and Tyr216 (activation). The GSK-3 Ser9 N-terminal domain can act as a false substrate, blocking substrate entry into the catalytic site and thereby inhibiting GSK-3 $\beta$  activity. Indeed, several drugs targeting GSK-3 $\beta$  have been developed. Alsterpaullone is a potent GSK-3 inhibitor to inhibit tau phosphorylation for the treatment of patients with advanced prostate cancer or Alzheimer's disease [13]. Tideglusib, a GSK-3 $\beta$  antagonist, is currently in a Phase IIb clinical trial for the treatment of Alzheimer's disease [14]. LiCl is a selective inhibitor of GSK-3 $\beta$  for the treatment of mania and depression [15]. These studies suggest that GSK-3 $\beta$  may be a promising drug target.

Based on the above, this study systematically explored the effects of DHA on CRC development through *in vitro* experiments and four animal models *in vivo*, including lung and peritoneal metastasis models, PDX model and AOM/DSS model. Moreover, we investigated the mechanism of DHA by transcriptome sequencing and identified the direct target. Importantly, a new therapeutic strategy of DHA in combination with Cap was proposed and its effects on CRC were investigated. Since existing chemotherapy combinations tend to cause immunosuppression and cumulative toxicity, we evaluated the safety, immunity and inflammatory responses of the combination of DHA and Cap. Above all, we systematically explored the effects and molecular mechanism of DHA in the development of CRC with the aim of providing an effective, low-toxicity drug and a new therapeutic strategy for the clinical treatment of CRC.

## 2. Materials and methods

### 2.1. Cell lines and animals

Human colorectal cell lines (HCT116, DLD-1, SW620, HCT-15), the murine colorectal carcinoma cell line (CT26 cells), the normal colon cell line (CCD18-C<sub>0</sub>) and human umbilical vein endothelial cells (HUVECs) were gifted from the department of Pathophysiology, Zhengzhou University. HCT116, DLD-1, HCT-15, SW620 and CT26 cells were cultured in RPMI-1640 medium (Biological Industries, Israel) with 10 % FBS (ScienCell, USA). CCD18-C<sub>0</sub> cells were cultured in MEM medium (Gibco, USA) supplemented with 10 % FBS, and HUVECs were cultured in endothelial cell medium (ECM) with 5 % FBS. These cells were cultured at 37 °C with 5 % CO<sub>2</sub>. Mice (CB17/SCID, BALB/c nude and BALB/c) were purchased from Beijing Charles River Laboratory Animal Technology and kept in the SPF level laboratory. The animal models were approved by the Ethics Committee of Zhengzhou University according to the guidelines of the Institutional Animal Care and Use Committee (ZZUIRB2023-299).

### 2.2. Cell proliferation assay

The CRC cells were plated in 96-well plates. After overnight cultivation, DHA (Meilunbio, Dalian, China) or Cap (MedChemExpress, Shanghai, China) was added to the medium. Then the cells were treated with drugs for 24 h, 48 h, 72 h or 96 h. Further, the cells were fixed with 4 % paraformaldehyde at room temperature for 30 min, and the cells were stained with 1 µg/mL DAPI for 20 min at 37 °C without light. Finally, the imaging analyser was used to count the number of cells.

### 2.3. Tumor sphere formation

The CRC cells were inoculated into each well (500 cells per well) of an ultra-low-attachment 96-well plate and supplemented with 100 µL RPMI-1640 medium, 2 % 1 × B27, 20 ng/mL human recombinant epidermal growth factor, 20 ng/mL basic fibroblast growth factor and 4 µg/mL insulin. The spheres were cultured at 37 °C with 5 % CO<sub>2</sub>. To calculate the forming efficiency, spheres with diameters > 50 µm were scored under a microscope after 5 days. The relevant primer sequences were listed in Table S1.

### 2.4. Transwell cell migration and invasion assays

The cells were pretreated with DHA for 24 h. The Matrigel was diluted with blank medium at a ratio of 1:6 (this step was only applicable to the invasion assay). And 70 µL Matrigel was placed in the chamber to solidify at 37 °C for 2 h. Then CRC cells (2 × 10<sup>4</sup> per well) were added to the upper layer in serum-free medium, and complete medium was added to the lower layer. The migration experiment was terminated 16 h later, and the invasion experiment was terminated 24 h later. The number of cells that invaded to the lower chamber was counted.

### 2.5. Induction of HUVECs and tube formation assay

HCT116 and DLD-1 cells were cultured at 80 % density and then incubated for 24 h with complete medium to collect the culture supernatant. Our previous studies have found that the characteristics of HUVECs induced by tumor conditioned medium (CM) were closer to those of tumor vascular endothelial cells [16]. The CM included 60 % culture supernatant of CRC cells and 40 % ECM medium, and then HUVECs were cultured with CM for 48 h. The Matrigel was spread in a 96-well plate to solidify at 37 °C for 2 h and cells (2 × 10<sup>5</sup> per well) were added. The cells were incubated for 2–4 h and photographed. The number of complete tubular lumen formations was counted.

### 2.6. Wound healing assay

CRC cells (2 × 10<sup>5</sup>/well) were seeded into 12-well plates. After reaching approximately 90 % confluence, the cell layer was scraped with a 10 µL pipette tip to create a wound. Then the cells were cultured in FBS-free medium with different drug concentrations and photographed with a microscope at specific times (0 h, 24 h, 48 h and 72 h). Finally, the wound closure was assessed using ImageJ software.

### 2.7. RNA extraction and qRT-PCR

Cells or tissues were sequentially extracted with Trizol, chloroform, isopropanol and 75 % ethanol in turn, and the enzyme-free water was used to solubilize the RNA. Genomic DNA isolation and reverse transcription were performed according to the kit (TaKaRa, Japan). The relevant primer sequences were listed in Table S1.

### 2.8. Transcriptome sequencing

HCT116 cells were treated with DMSO or 30 µM DHA for 24 h, then the cells were lysed with Trizol and the cell lysate was collected.

Qualified total RNA was selected as the initial sample for mRNA sequencing. Transcriptome sequencing was completed by CapitalBio Technology (Beijing, China), and the *P*-value < 0.05 and  $|\text{Log2FC}| \geq 1$  were set as the thresholds to identify the differentially expressed genes.

### 2.9. Molecular docking simulation of the interaction of DHA and GSK-3 $\beta$

Molecular docking and molecular dynamics (MD) simulations were performed to construct and optimize the binding complex structure of DHA (PubChem ID: 3000518) with GSK-3 $\beta$  (PDB ID: 4NMO) [17]. Initially, DHA was docked into the possible active site of the enzyme by AutoDock 4.2 program (RRID: SCR\_012746) [18]. After the initial model was prepared, the ionizable residues were set to the standard protonated or deprotonated states at the physiological conditions ( $\text{pH} = \sim 7.4$ ). The complex structure was solvated in a rectangular box of TIP3P water molecules with a minimum solute-wall distance of 10 Å. Additional Cl $^-$  was added in the solvent as counter ions to neutralize the whole system. In the following, a series of energy minimizations were carried out by using the PMEMD module of Amber 16 program with a non-bonded cut off of 10 Å and a conjugate gradient energy-minimization method. Next, the two systems were gradually heated from 10 to 298.15 K by weak-coupling method with a constraint force constant of 5 kcal mol $^{-1}$ . The constraint force constant was gradually decreased during a period of 2 ns equilibration and finally removed for the production MD simulation. To obtain a stable MD trajectory, the production MD simulation was kept running 20.0 ns in the NTP ensemble, at  $T = 298.15$  K. Afterwards, the representative snapshots of the complex structure was extracted from the production MD.

### 2.10. Western blotting

The cells and tissues were lysed in RIPA lysate buffer. Then the proteins were separated by SDS-PAGE and transferred to PVDF membranes. The membranes were blocked with 5 % non-fat milk and incubated with primary antibodies at 4 °C overnight. The antibodies used in this study were as follows: Ki67 (Santa Cruz, USA, Cat#SC23900, 1:200, RRID: AB\_627859); CD31 (Abcam, USA, Cat#ab9498, 1:500, RRID: AB\_307284);  $\beta$ -catenin (Abcam, USA, Cat#ab32572, 1:5000, RRID: AB\_725966); TCF7 (for western blotting: Wanleibio, Shenyang, China, 1:500; for Co-IP: Cell Signaling Technology, Cat#2203, USA, 1:750, RRID: AB\_2199302); p-GSK-3 $\beta$  (Ser9) (Wanleibio, Shenyang, China, WL03683, 1:500); GSK-3 $\beta$  (Wanleibio, Shenyang, China, WL01456, 1:500); MMP9 (Affinity Biosciences, China, 1:500, AF5228, RRID: AB\_2837714); GAPDH (ZSGB-Bio, China, Cat#TA-08, 1:1000, RRID: AB\_2747414). After that, the membranes were incubated with the corresponding secondary antibodies at room temperature for 2 h. Finally, the protein bands were visualized by ECL reagent (Beyotime, China).

### 2.11. Human angiogenic factor antibody microarray assay

The human angiogenic factor antibody microarray was purchased from R&D Systems (ARY007). HCT116 cells were seeded in six-well plates at a density of  $1.5 \times 10^5$  cells/mL with DMSO or 30  $\mu\text{M}$  DHA for 24 h, then the supernatant was collected. The antibody microarray was placed in Array buffer 7 and incubated at room temperature for 1 h. 0.5 mL of the supernatant, 50  $\mu\text{L}$  of Detection Antibody Cocktail and 0.5 mL of Array Buffer 4 were mixed to incubate for 1 h. The antibody microarray was incubated with the mixture overnight at 4 °C. After washing with Wash Buffer, the microarray was incubated with Streptavidin-HRP for 30 min at room temperature. Chemi Reagent Mix was used for exposure, development and fixation.

### 2.12. Coimmunoprecipitation (Co-IP) assay

The cells were added to pre-cooled RIPA and placed on ice for lysis for 30 min. After centrifugation, the concentration of the supernatant

was measured by BCA. 2 mg of total protein was supplemented to 500  $\mu\text{L}$  with RIPA. The TCF7 antibody was mixed with the protein and incubated overnight at 4 °C. RIPA was used to wash magnetic beads (25  $\mu\text{L}$ ). The beads were then mixed with the immunoprecipitation mixture and incubated for 2 h. 100  $\mu\text{L}$  of 1 × loading buffer was used to elute the proteins and incubated at 100 °C for 10 min. Further, the supernatant containing the target protein was retained and analyzed by western blotting.

### 2.13. Chromatin immunoprecipitation (ChIP) assay

The cells were coincubated with 37 % formaldehyde and medium to cross-link chromatin with proteins. Glycine, micrococcal nuclease, ChIP buffer and PIC (ChIP kit, CST, USA) were added in turn for ultrasonic lysis, and the supernatant was the cross-linked chromatin preparation. TCF7 antibody or IgG was added to the diluted chromatin overnight. Magnetic beads were mixed with the sample at 4 °C for 2 h. Low-salt and high-salt solutions were used to wash the sediment. Chromatin was eluted with ChIP buffer, and the cross-linking was broken by 5 M NaCl and Proteinase K at 65 °C for 2 h. DNA was purified and the promoter regions for the MMP9 were detected by qRT-PCR. Besides, the binding sites of TCF7 on the promoter regions of MMP9 were found by JASPAR database. The four primer sequences for the binding sites were shown in Table S2.

### 2.14. Dual-Luciferase reporter assay

Four reporter gene plasmids (Sangon Biotech, Shanghai, China) were designed for the promoter region of MMP9 based on the result of ChIP assay. Then, 1  $\mu\text{g}$  pcDNA3.1-Flag-TCF7 plasmid (Unibio, Changsha, China, RRID: Addgene\_79663), 1  $\mu\text{g}$  luciferase reporter plasmids (Firefly luciferase) and 50 ng pRL-TK vector (Renilla luciferase) (RRID: Addgene\_11313) were transfected into HCT116 cells with 200  $\mu\text{L}$  jetPrimer buffer and 4  $\mu\text{L}$  jetPrimer (Polyplus, France) for 48 h. The reporter activity was measured by Dual Luciferase Assay (E1910, Promega, USA). The supernatant was used to detect Firefly luciferase (Rlu1) and Renilla luciferase (Rlu2) activity, and Rlu1/Rlu2 was calculated as the final result.

### 2.15. Pull down assay

Sepharose 4B (GE Healthcare, USA) was activated with 1 mM HCl and incubated with DMSO or DHA (4 mg) and coupling buffer at 4 °C for two nights. Then the beads were incubated with 0.1 M Tris-HCl buffer at 4 °C overnight. Further, the beads were washed twice with 0.1 M Acetate buffer and 0.1 M Tris HCl-0.5 M NaCl. The beads were mixed with PBS. Cell lysate (1 mg) was incubated with beads at 4 °C for two nights. The beads were washed and the proteins were boiled in 4 × loading buffer at 95 °C for 5 min. Then the protein expression levels were detected by western blotting.

### 2.16. Immunohistochemical staining of tissue microarray of patients

Human CRC tissue microarray was purchased from Outdo Biotech Company (Shanghai, China) with the ethical approval (SHYJS-CP-1701008). Inclusion criteria: ① pathological diagnosis of colorectal adenocarcinoma; ② receiving radical or partial colorectal resection. Exclusion criteria: ① receiving preoperative radiotherapy and chemotherapy; ② lack of pathological information. A total of 71 patients were included in this study and tumor and paracancerous tissues were collected from each patient. Due to problems with section location and some detachments, 71 tumor tissues and 53 paracancerous tissues were finally available. The expressions of p-GSK-3 $\beta$  (Ser9) in CRC tissues ( $n = 71$ ) and paracancerous tissues ( $n = 53$ ) were detected by immunohistochemical staining (IHC). The number of p-GSK-3 $\beta$  (Ser9) positive cells and staining intensity were converted into numerical values using the

internationally recognized H-score scale. According to the calculation formula: H-score = 1 × weak staining + 2 × moderate staining + 3 × strong staining (weak, moderate and strong staining represent the number of positive cells as a percentage of the total number of cells in the section). After ROC curve analysis, H = 104.15 was selected as the cut-off point to analyze the protein level of p-GSK-3β (Ser9) in tissues. Finally, the relationship between the expression of p-GSK-3β (Ser9) and the pathological data of the patients was analyzed.

### 2.17. Lymphocytes extraction from spleen and tumor

The spleen of the mouse was gently combed with a forcep to release the splenocytes. The spleen was then crushed on a sieve using a syringe tip. The cell suspensions were rinsed with PBS, collected into EP tubes and centrifuged at 450 g for 5 min. Erythrocyte lysate was used to remove erythrocytes at room temperature for 2 min. 10 mL of PBS was used to terminate the lysis. Next, the cell suspensions were centrifuged at 1500 rpm for 5 min. PBS containing 10 % FBS was used to resuspend the cell precipitate. The single positive tubes (CD8<sup>+</sup> or CD3<sup>+</sup>) and double positive tubes (CD8<sup>+</sup>CD3<sup>+</sup>) were set up respectively. The corresponding antibodies (PE-anti-mouse-CD8a, Biolegend, China, Cat#100708, RRID: AB\_312747; FITC-anti-mouse-CD3a, Biolegend, China, Cat#100306, RRID: AB\_312671) were added to the cells and incubated for 1 h at room temperature in darkness. The cells were washed again with PBS containing 10 % FBS and the results were analyzed using a flow cytometer.

### 2.18. GSK-3β (Ser9) inactivation mutation assay

The pcDNA3.1-Flag-GSK-3β (Ser9A) plasmid (Unibio, Changsha, China) has the inactivated GSK site with a mutation of the GSK serine 9 residue to alanine. HCT116 cells were placed in six-well plates at a density of  $2 \times 10^5$  cells per well, transfected with GSK-3β (Ser9A) or empty vector (pcDNA3.1) for 48 h and then examined by western blotting.

### 2.19. Animal models

**Patient-derived xenografts (PDX) model**—CRC tissues (HJG224 and HJG259) were obtained from the Affiliated Cancer Hospital of Zhengzhou University. CRC tissues were transplanted into the axilla of CB17/SCID mice (female, 6–8 weeks old) near the left upper limb. After four consecutive transplants, the tumor tissues were inoculated subcutaneously into the mice. DHA and Cap were dissolved in 10 % DMSO and 90 % corn oil. When the tissue grew to 50–80 mm<sup>3</sup>, the mice were randomly divided into 4 groups ( $n = 10$ ): solvent control group, 30 or 60 mg/kg DHA group (i.p.) and 359 mg/kg Cap positive group (i.g.). The drugs were administered in a cycle of two weeks on and one week off, corresponding to the clinical administration and dose of Cap [19]. The organs (heart, liver, spleen, lung and kidney) were harvested for organ index calculation and to do the haematoxylin and eosin (HE) staining. Tumor volume (mm<sup>3</sup>) = (long diameter) × (short diameter)<sup>2</sup> × 0.5.

**Metastasis models**—CT26 cells ( $8 \times 10^5$ ) were injected into the tail vein of BALB/c mice to establish the lung metastasis model. HCT116 cells ( $2 \times 10^6$ ) were injected into the tail vein of BALB/c nude mice to establish the peritoneal metastasis model. The day after cell injection, the mice were divided into 4 groups ( $n = 10$ ). The treatment was the same as in the PDX model.

**AOM/DSS model**—The BALB/c mice (female, 8 weeks old) were divided into 5 groups: normal group, AOM/DSS model group, 30 mg/kg DHA group, 359 mg/kg Cap group and the combination group ( $n = 12$ ). On the first day, mice were injected intraperitoneally with 10 mg/kg azoxymethane (AOM, Sigma-Aldrich, USA), followed by regular diet and water for two weeks. Further, mice were administered with four cycles of 2 % dextran sodium sulfate (DSS, MP biomedical, USA) for 7 days and drinking water for 14 days. The lymphocytes were extracted from

the spleen and tumor to detect the effect of DHA on immunity and inflammation.

### 2.20. Statistical analyses

GraphPad Prism 8.0 (RRID: SCR\_002798) and SPSS 22.0 (RRID: SCR\_002865) software were used for data analysis. The *t*-test was used to compare two groups of samples, and one-way ANOVA was used to compare multiple groups of samples. The matched-pair analysis was used to analyze the expression of p-GSK-3β (Ser9) in tumor tissues and precancerous tissues.  $P < 0.05$  was considered statistically significant.

## 3. Result

### 3.1. DHA inhibits the proliferation, stemness, metastasis and angiogenesis of CRC

To explore the cytotoxicity of DHA on human CRC cells (HCT116, DLD-1, HCT-15 and SW620) and normal colon cells (CCD-18C<sub>0</sub>), we first designed the cytotoxicity assays. The results showed that DHA was significantly toxic to CRC cells, while DHA was less toxic to CCD-18C<sub>0</sub>. Moreover, DHA significantly inhibited the proliferation of CRC cells (Fig. 1A–C). Colony formation rate is an important index of cell population dependency and proliferation. Here we found that DHA effectively suppressed the anchorage-independent and unanchored-independent growth of CRC cells (Fig. 1D).

As known, tumor stem cells are a group of cells with self-renewal ability, which play an important role in tumor survival, proliferation, metastasis and recurrence [20]. To investigate whether DHA affects the stemness of CRC cells, we performed tumor sphere formation and checked the stem cell surface markers. The results showed that DHA could inhibit the tumor sphere formation (Fig. 1E). In addition, DHA inhibited the mRNA expression of stem cell surface markers (CD133, CD44, Nanog and OCT4) as well as the protein expression of Nanog (Fig. S1).

Furthermore, DHA significantly inhibited the migration and invasion of CRC cells (Fig. 1F). Inhibition of angiogenesis is an effective strategy to inhibit the development of tumor [21]. Under physiological conditions, endothelial cells are almost quiescent, with only about 0.1 % of endothelial cells proliferating [22]. HUVECs are widely used in the research of tumor angiogenesis due to their rapid proliferative capacity [23]. Our previous studies have shown that the characteristics of HUVECs induced by tumor conditioned medium (CM) are more closely resemble those of tumor vascular endothelial cells [16,24]. Herein, DHA strongly inhibited the migration, invasion and tube formation of HUVECs induced by HCT116 and DLD-1 CM (Fig. 1G and H, Figs. S2–S4).

Further, to explore the role of DHA on CRC metastasis *in vivo*, CT26 cells were injected into mice via the tail vein. After 14 days, significant lung metastases were observed, spreading throughout the lungs and increasing in size and weight. Notably, 60 mg/kg DHA achieved almost the same inhibitory effect as the Cap-positive group (Fig. 1I–K). Moreover, lung metastases caused rapid weight loss in mice in the control group, while the mice in the 60 mg/kg DHA group had the most stable weight (Fig. 1L, Fig. S5). Taken together, DHA showed strong inhibition of CRC proliferation, metastasis and angiogenesis.

### 3.2. DHA inhibits Wnt/β-catenin/TCF7/MMP9 signaling pathway in CRC cells

To further explore the key signaling pathway of DHA in inhibiting the development of CRC, HCT116 cells were treated with 30 μM DHA for 24 h for transcriptome sequencing (Fig. 2A, Fig. S6). Then, KEGG analysis showed that the canonical Wnt/β-catenin pathway might play a key role in DHA-induced inhibition of CRC development (Fig. 2B). Furthermore, GSEA analysis also indicated that Wnt signaling pathway

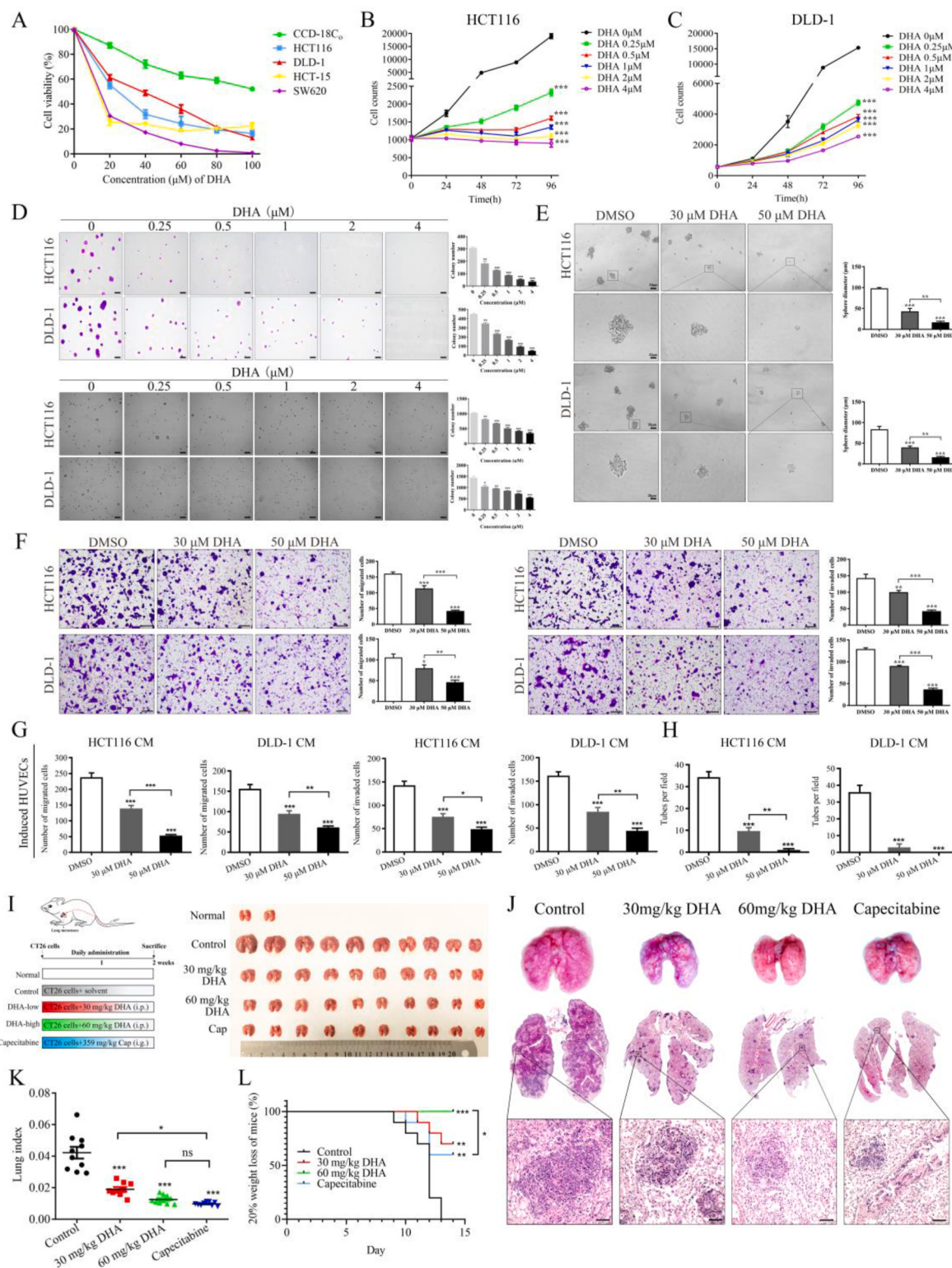


**Fig. 1. DHA inhibits the proliferation, colony formation, tumor sphere formation, migration, invasion, angiogenesis and lung metastasis in CRC.** (A) Cytotoxicity assay detected the cell viability of colorectal cell lines (HCT116, DLD-1, HCT-15, SW620) and normal colon cells (CCD18-C<sub>0</sub>) treated with DHA for 48 h. (B–C) Proliferation assay examined the number of surviving CRC cells with DHA treatment. (D) Plate cloning assay and soft agar cloning assay detected the effects of DHA on the anchorage-independent and unanchored-independent growth of CRC cells. (E) The effects of DHA on tumor sphere formation of CRC cells. (F) The effects of DHA on the migration and invasion of CRC cells. (G–H) The statistics of the effects of DHA on migration, invasion and tube formation of CRC cells CM-induced HUVECs. (I–J) Schematic diagram and representative lung metastases in the CT26 lung metastasis model (n = 10). (K) The statistics of lung index. Lung index = lung weight/body weight (L) The survival curve was plotted with 20 % weight loss of mice as the inflection point. The results were presented as the mean  $\pm$  S.D. of three independent experiments. (\*P < 0.05, \*\*P < 0.01, \*\*\*P < 0.001).

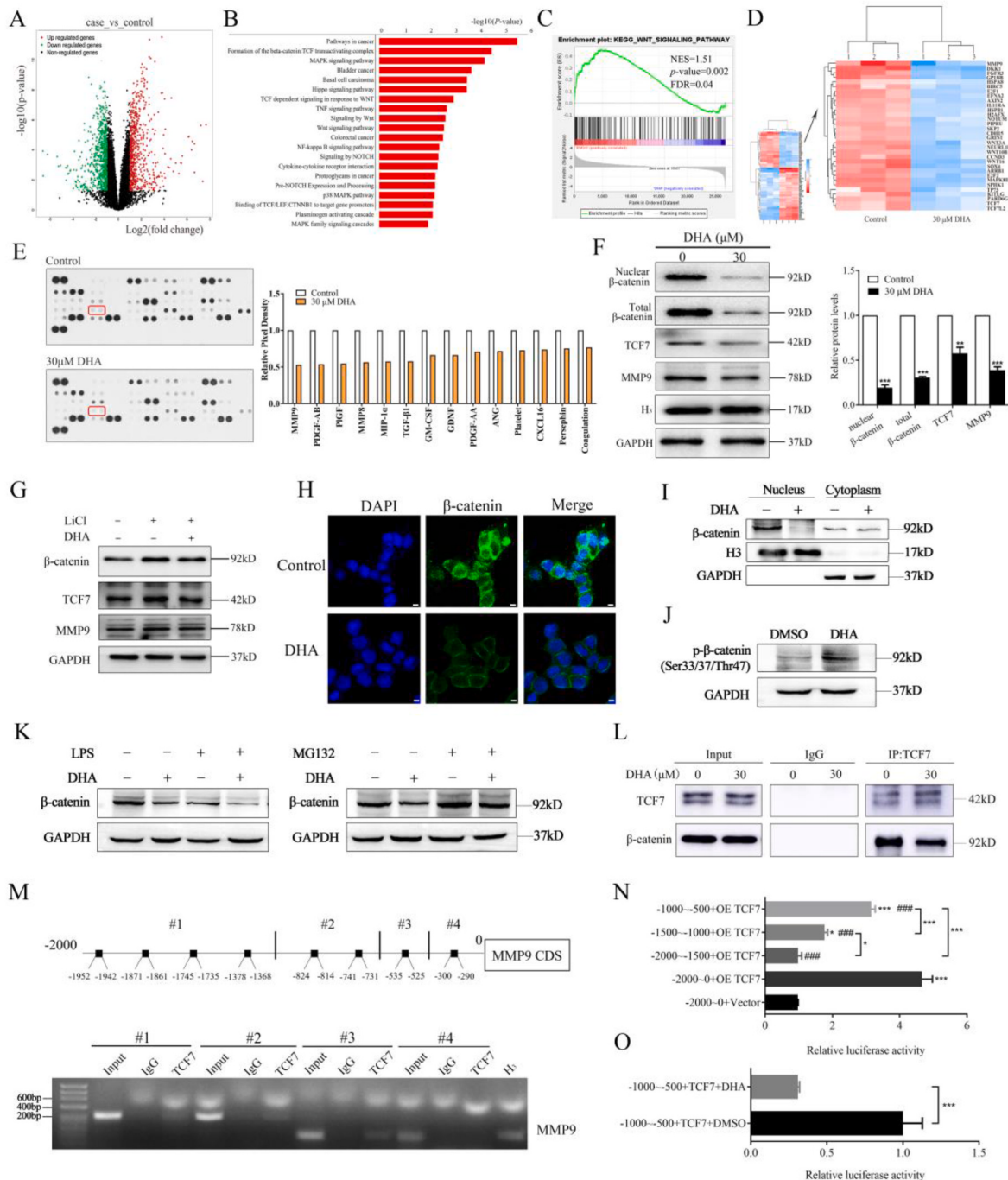


**Fig. 2. DHA inhibits Wnt/β-catenin/TCF7/MMP9 signaling pathway in CRC.** (A) The changes of mRNA with 30 μM DHA treatment for 24 h were identified by RNA-seq.  $P$ -value  $< 0.05$  and  $|Log2FC| \geq 1$  was set to the threshold. (B) The top 20 signaling pathways with DHA treatment. (C) GSEA analysis showed the effect of DHA on Wnt signaling pathway. (D) The genes from the top 20 signaling pathways ranked by fold change. (E) The changes of angiogenic factors with DHA treatment by human angiogenic factor antibody microarray. MMP9 was marked with the red box. (F) The effect of DHA treatment for 24 h on the expression levels of TCF7, β-catenin and MMP9 in HCT116 cells ( $n = 3$ ). H3 was used as the nuclear reference. (G) The effects of DHA on β-catenin, TCF7 and MMP9 protein levels after LiCl pretreatment were detected by western blotting ( $n = 3$ ). (H) The effect of DHA on the localization of β-catenin was detected by immunofluorescence assay. (Scale bar = 25 μm) (I) The effect of DHA on the expression level of β-catenin in the nucleus and in cytoplasm. (J) The effect of DHA on the expression level of p-β-catenin (Ser33/37/Thr47) in HCT116 cells. (K) The effects of 200 ng/mL LPS or 20 μM MG132 combined with DHA on the expression level of β-catenin. (L) Co-IP assay detected the effect of DHA treatment for 2 h on the binding of β-catenin and TCF7 ( $n = 3$ ). (M) The binding sites of TCF7 on the promoter regions of MMP9 were found in JASPAR. ChIP assay was used to detect the binding. (N) Dual-luciferase reporter gene assay detected the transcriptional activity of TCF7 on MMP9. (O) Dual-luciferase reporter gene assay detected the transcriptional activity of TCF7 on MMP9 with DHA treatment. (\*\* $P < 0.01$ , \*\*\* $P < 0.001$ , ### $P < 0.001$  VS -2000~0+OE TCF7).

was significantly inhibited by DHA (Fig. 2C). In addition, the transcription factor TCF7 was found to be most frequently enriched in Wnt-related signaling pathways (Table S3). Moreover, cluster analysis revealed that the mRNA level of MMP9 changed the most among all down-regulated genes (Fig. 2D). Since angiogenesis is closely related to tumor progression, we detected the changes of angiogenic factors. Coincidentally, MMP9 was the most significantly down-regulated angiogenic factor (0.53-fold change) after DHA treatment (Fig. 2E). Therefore, we hypothesized that DHA inhibited the development of CRC by Wnt/β-catenin/TCF7/MMP9 signaling pathway.

To verify this hypothesis, we first detected the changes in related molecules at the mRNA and protein levels firstly. DHA significantly inhibited the expression levels of TCF7, MMP9, nuclear and total β-catenin (Fig. 2F, Fig. S7). Moreover, DHA reduced the levels of β-catenin, TCF7 and MMP9 that were increased by LiCl (the agonist of Wnt/β-catenin pathway) (Fig. 2G). Furthermore, nucleation of β-catenin is crucial for the activation of Wnt/β-catenin pathway. Immunofluorescence assay showed that DHA inhibited nuclear entry of β-catenin (Fig. 2H and I). Moreover, we explored the effect of DHA on β-catenin ubiquitination. DHA increased the expression of p-β-catenin Ser33/37/Thr47 (Fig. 2J). Further, the ubiquitin-proteasome agonist LPS promoted DHA-induced degradation of β-catenin, and the ubiquitin-proteasome inhibitor MG132 inhibited DHA-induced degradation of β-catenin (Fig. 2K). Above all, DHA inhibited the entry of β-catenin into the nucleus and induced its ubiquitinated degradation in the cytoplasm in CRC cells. In addition, DHA was proved to inhibit the binding of β-catenin to TCF7 by Co-IP assay, where DHA treatment for 2 h did not alter the expression levels of β-catenin and TCF7 (Fig. 2L, Fig. S8). Besides, 8 binding sites for TCF7 in the promoter regions of MMP9 were identified by JASPAR database, thus we designed four primer sequences for the binding sites (Fig. 2M). ChIP assay identified that the first three segments of the MMP9 promoter region may contain TCF7 binding sites. Dual-luciferase reporter gene assay showed that the region of -1000 bp ~ -500 bp was the main binding region, and DHA significantly reduced the transcription regulation of TCF7 on MMP9 (Fig. 2N and O). Collectively, our findings preliminarily suggested that DHA inhibited Wnt/β-catenin/TCF7/MMP9 pathway in CRC cells.

### 3.3. GSK-3β is the direct target of DHA

In order to explore the target of DHA, we first made predictions in Herb and Swisstarget databases, and jointly predicted 8 targets (Fig. 3A). Among these, GSK-3β was a key regulatory kinase of Wnt signaling pathway. Herein, molecular docking and molecular dynamics simulations were first performed to predict the binding pattern of DHA to GSK-3β. It was obvious that RMSD values for the complex and DHA were all convergent with the average values of ~1.5 Å (Fig. 3B). Specifically, the hydroxyl group formed hydrogen bonds with the backbone of Val135 and Glu137 via a water bridge, and the sidechain of Arg141 was also hydrogen-bonded with the epoxy group of DHA. In addition, the three fused rings of DHA formed extensive hydrophobic interactions with the side chains of Ile62, Phe67, Val70, Ala83, Lys85, etc (Fig. 3C). The representative snapshot of the binding complex showed that DHA fit well into the binding pocket. On this basis, the pull down assay demonstrated that DHA bound directly to GSK-3β (Fig. 3D). In addition, other signaling pathways normally involved in GSK-3β, such as PI3K-AKT pathway and NF-κB signaling pathway, were not significantly changed after DHA treatment (Fig. S9), which also indicated the specific inhibition of Wnt pathway in CRC by DHA through targeting GSK-3β. Furthermore, DHA did not affect the mRNA and protein level of GSK-3β, while it significantly inhibited the protein level of p-GSK-3β (Ser9) (Fig. 3E and F, Fig. S10). Besides, p-GSK-3β (Ser9) and MMP9 were highly expressed in tumor tissues and they were positively correlated in 9 pairs of CRC samples (Fig. 3G, Fig. S11). In larger samples, the expression level of p-GSK-3β (Ser9) was significantly higher in human colorectal adenocarcinoma tissues ( $n = 71$ ) than in precancerous tissues

( $n = 53$ ), as well as in 47 paired samples (Fig. 3H–J). Significantly, p-GSK-3β (Ser9) was positively correlated with the depth of invasion and clinical stage (Table 1), implying that p-GSK-3β (Ser9) is a potential biomarker for local infiltration and tumor progression in CRC.

To further clarify the targeting role of DHA on GSK-3β in CRC development, we designed the GSK-3β (Ser9) inactivation mutation assay by mutating GSK serine 9 residue to alanine (Fig. 3K). The results showed that the inhibition of proliferation and migration of CRC cells by DHA was significantly attenuated by inactivation of Ser9 of GSK-3β (Fig. 3L-N). In addition, LiCl, a specific inhibitor of GSK-3β, was used to confirm the targeting role of DHA on GSK-3β. The inhibitory effects of DHA on proliferation, migration, invasion and angiogenesis of HCT116 cells were weakened after pretreatment with LiCl, as were those of HUVECs induced by HCT116 CM (Fig. 3O-Q, Figs. S12-S13). Above all, DHA directly targeted GSK-3β to inhibit the development of CRC.

### 3.4. DHA inhibits the growth of CRC by GSK-3β/TCF7/MMP9 pathway

To further validate the effect of DHA on CRC growth *in vivo*, we constructed the PDX model to comprehensively assess the drug efficacy and safety. A significant correlation between patient drug response and the corresponding PDXs was observed in over 87 % of clinical treatment outcomes [25]. Two CRC tissues from patients (No. HJG224 and HJG259) with GSK-3β/TCF7/MMP9 pathway activation were selected to conduct PDX models (Fig. 4A and B, Fig. S14). In both of the two PDX models, DHA significantly inhibited the tumor growth. Importantly, 60 mg/kg DHA achieved almost the same inhibitory effect as Cap (Fig. 4C and D). Besides, DHA inhibited the expression levels of Ki67, CD31, p-GSK-3β (Ser9), β-catenin, TCF7 and MMP9 (Fig. 4E and F). There were no significant differences in the body weight, temperature and organ index, except for an increase in spleen index in DHA group (Fig. 4G and H, Table S4). The increase in spleen index may be due to the enhanced immunity to DHA. HE staining showed no obvious morphological abnormalities in the organs of mice treated with DHA, whereas the renal tubules of mice in Cap group were slightly dilated, accompanied by an increase in renal index (Fig. 4I). Similar results were also observed in HJG259 PDX model (Figs. S15-S16, Table S5). Overall, DHA inhibited the growth of CRC by GSK-3β/TCF7/MMP9 pathway, with no significant toxic and side effects at the doses within 60 mg/kg.

### 3.5. The combination of DHA and Cap synergistically inhibits the development of CRC

As known, Cap-based combination strategies such as CapeOx (Cap + oxaliplatin) and CapIRI (Cap + irinotecan) are widely used in the clinic. However, CapeOx therapy was reported to cause severe gastrointestinal toxicity, which ultimately led to dose limitation [26]. Based on this, we further explored whether the combination of DHA and Cap could improve the efficacy or even reduce side effects. Firstly, we selected 1 mM Cap and 30 μM DHA as the combination concentration for further experiments based on the toxicity assay and the combination index (CI) (Fig. 5A, Fig. S17). The combination showed a better inhibitory effect on the proliferation, migration and invasion of CRC cells than that of the single drug (Fig. 5B and C), and the tube formation was almost completely inhibited by the combination (Fig. 5D). Furthermore, HCT116 cells were injected into the tail vein of nude BALB/c mice through to explore the effect of the combination of DHA and Cap on CRC metastasis *in vivo*. The metastases were distributed in the abdominal wall, intestinal wall, lesser omentum, mesentery and diaphragm (Fig. 5E). Moreover, the stable body weight indicated that this combination had a good safety (Fig. 5F). Compared with the control group, both DHA and Cap significantly inhibited the total number of metastases (Fig. 5G and H). Taken together, DHA combined with Cap had a better inhibitory effect on CRC proliferation, metastasis and angiogenesis than either drug alone.

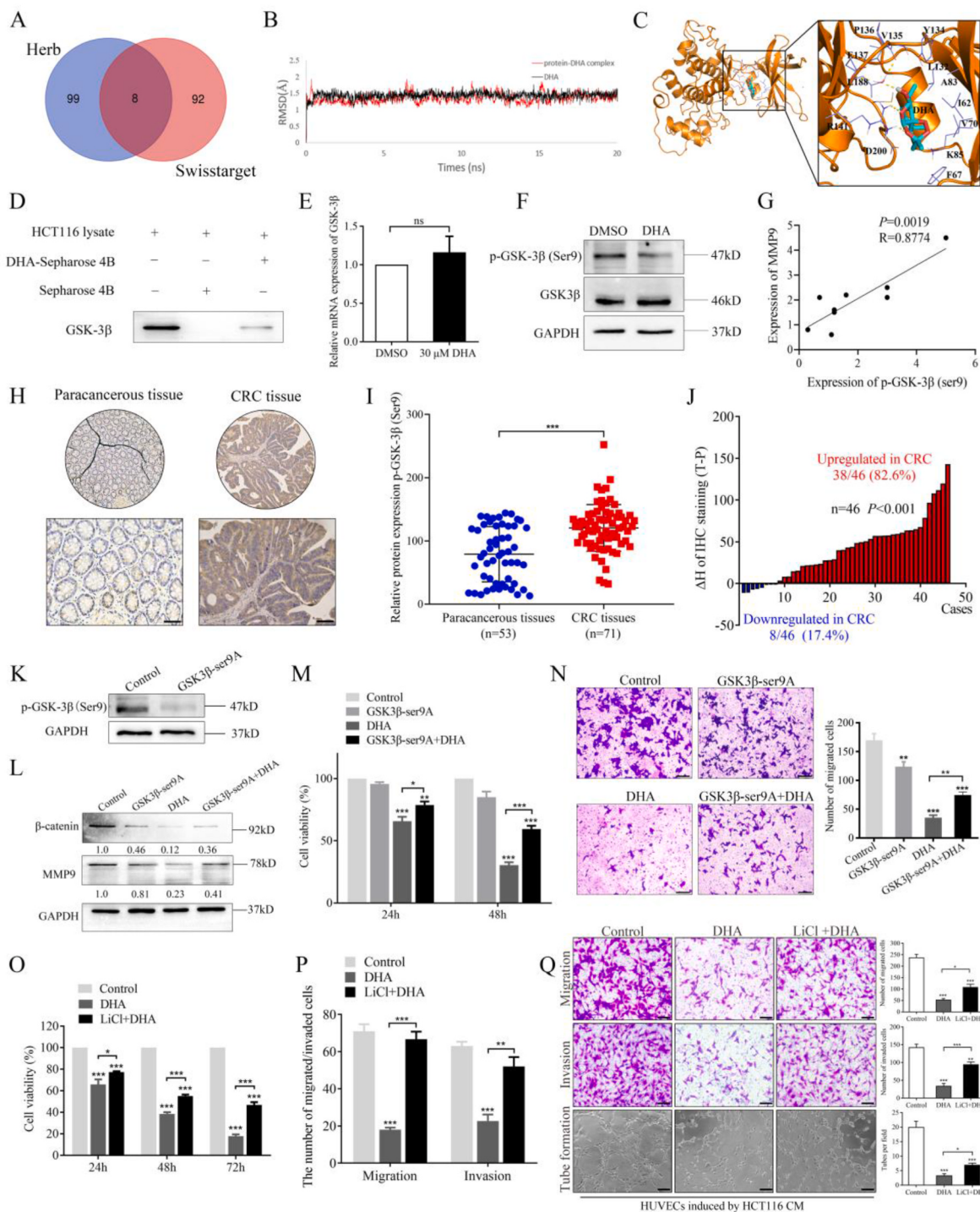


**Fig. 3. DHA directly targets GSK-3β to inhibit the development of CRC cells.** (A) Venn chart showed the predicted targets of DHA in Herb and SwissTarget databases. (B) RMSD values of GSK-3β-DHA complex (red) and DHA (black) during 20 ns MD simulations. (C) Representative binding complex structure of DHA (stick, cyan) and GSK-3β (cartoon, saffron yellow) derived from MD simulations. The residues interacting with DHA were shown as purple lines. (D) Pull down assay detected the binding of DHA and GSK-3β. (E) The mRNA level of GSK-3β changed by DHA. (F) The effect of DHA on the protein levels of p-GSK-3β (Ser9) and GSK-3β. (G) The correlation between the expressions of p-GSK-3β (Ser9) and MMP9 in 9 pairs of CRC samples. (H-I) The pathological figures and statistics showed the expression of p-GSK-3β (Ser9) in CRC tissues and paracancerous tissues. (Scale bar = 50 μm) (J) The expression of p-GSK-3β (Ser9) in 46 pairs of CRC samples. (K) The mutation efficiency of p-GSK-3β (Ser9) in HCT116 cells. (L) The effect of DHA on the expression levels of β-catenin and MMP9 with p-GSK-3β (Ser9A). (M) The cell viability of HCT116 cells with p-GSK-3β (Ser9A) after DHA treatment for 48 h. (N) The migration ability of HCT116 cells with p-GSK-3β (Ser9A) after DHA treatment for 24 h. (O-P) The effect of DHA treatment for 24 h on the proliferation, migration and invasion of HCT116 cells pretreated with 20 μM LiCl for 1 h. (Q) The effect of DHA treatment for 24 h on the migration, invasion and tube formation ability of CM-induced HUVECs pretreated with 20 μM LiCl for 1 h. The results were shown as the mean ± S.D. of three independent experiments. Scale bar = 100 μm. (\*P < 0.05, \*\*P < 0.01, \*\*\*P < 0.001).

**Table 1**

Correlation between the expression of p-GSK-3 $\beta$  (Ser9) and the clinicopathological parameters of the patients.

Characteristics	p-GSK-3 $\beta$ (Ser9) expression levels (n = 71 cases)		
	Low (n = 20)	High (n = 51)	P
Age (years)			
≤60	7 (35.0 %)	18 (35.3 %)	
>60	13 (65.0 %)	33 (64.7 %)	0.981
Gender			
Males	10 (50.0 %)	31 (60.8 %)	
Females	10 (50.0 %)	20 (39.2 %)	0.408
Depth of invasion			
T1	2 (10.0 %)	0 (0.0 %)	
T2	3 (15.0 %)	2 (3.9 %)	
T3	5 (25.0 %)	20 (39.2 %)	
T4	10 (45.0 %)	29 (56.9 %)	0.03*
Lymph node metastasis			
N0	15 (75.0 %)	33 (64.7 %)	
N1	5 (25.0 %)	15 (29.4 %)	
	0 (0.0 %)	3 (5.9 %)	0.472
Distant metastasis			
M0	18 (90.0 %)	49 (96.1 %)	
M1	2 (10.0 %)	2 (3.9 %)	0.314
Clinical stage			
I	5 (25.0 %)	2 (3.9 %)	
II	10 (50.0 %)	30 (58.9 %)	
III	3 (15.0 %)	17 (33.3 %)	
IV	2 (10.0 %)	2 (3.9 %)	0.025*
Tumor diameter			
≤5 cm	12 (60.0 %)	28 (54.9 %)	
>5 cm	8 (40.0 %)	23 (45.1 %)	0.697
Differentiation			
Poor	16 (80.0 %)	48 (94.1 %)	
Moderate/High	4 (20.0 %)	3 (3.9 %)	0.051

### 3.6. The combination of DHA and Cap inhibits colitis-associated colorectal cancer

Colitis-associated cancer (CAC) is a specific form of CRC. One study reported a 20-fold increased risk of CRC in patients with ulcerative colitis, and a 3-fold increased risk of CRC in patients with Crohn's disease [27]. More importantly, recent evidence also implicates inflammation is present at the onset of sporadic and familial CRC [28]. Hence, the AOM/DSS model was conducted to examine the effect of DHA on CAC (Fig. 6A). We observed that the body weight of the mice dropped due to diarrhoea during the feeding of DSS, whereas the weight of mice in DHA and combination groups was more stable. Meanwhile, the mice in Cap group lost much of their body weight due to severe diarrhoea (Fig. 6B, Figs. S18–S19). Furthermore, the length of colon was significantly shortened in control group, suggesting inflammatory injury. DHA and the combination restored the length of colon. However, Cap resulted in the shortest colon length, which was associated with underlying inflammation and severe diarrhoea (Fig. 6C). HE staining showed the malformed crypts, irregular and hyperplastic glands, abnormally thickened mucosa and colorectal adenomas in control group. In contrast, both of DHA and Cap were able to reverse some of the damage. Importantly, the combination had a regular and uniform arrangement of gland sizes and significantly reduced inflammatory infiltration (Fig. 6D). However, Cap increased infiltrating immune cells, which may be due to the increased inflammation leading to immune cell recruitment. Indeed, the combination performed a better inhibitory effect on the number and volume of tumor in colon (Fig. 6E). To our surprise, the tumors also appeared in the small intestine, and Cap increased the number of tumors in small intestine compared with the control group. Meaningfully, this combination reduced the number of small intestine tumor increased by Cap (Fig. 6F and G). Besides, this combination had no apparent toxicity to the mice according to the organ index (Fig. 6H). Moreover, we verified that DHA effectively inhibited GSK-3 $\beta$ /TCF7/MMP9 pathway in CRC tumor (Fig. 6I and J). These

findings indicated that the combination of DHA and Cap showed a better inhibitory effect on CAC with good safety and reduced side effects caused by Cap.

### 3.7. The combination alleviates the immunosuppression and inflammation caused by Cap

As Cap has been reported to have immunosuppressive and pro-inflammatory effects, thus we further investigated the effects of the combination of DHA and Cap on immunity and inflammation. In this study, the animal models in DHA group showed a significant increase in spleen volume and index (Fig. 7A and B, Fig. S20), which drew our attention to the effect of DHA on immune function. At first, we detected the number of CD8 $^{+}$ CD3 $^{+}$ T cells of spleen. In both of the two models, DHA significantly increased the number of CD8 $^{+}$ CD3 $^{+}$ T cells in spleen, while Cap decreased it. In particular, the combination increased the number of CD8 $^{+}$ CD3 $^{+}$ T cells in the spleen (Fig. 7C and D). More deeply, the number of CD8 $^{+}$ CD3 $^{+}$ T cells in colon tumor was further detected (Fig. 7E). The control group showed a decrease in the number of CD8 $^{+}$ CD3 $^{+}$ T cells in tumor, while DHA and the combination rescued it to some extent. However, Cap led to the greatest increase in CD8 $^{+}$ CD3 $^{+}$ T cells in tumor (32.8 %), which could be due to being in an acute bleeding phase [29]. Furthermore, the immunopotentiating factor IFN- $\gamma$  and the immunosuppressive factor TGF- $\beta$  in tumor were also detected to assess immune infiltration. DHA increased the level of IFN- $\gamma$  and decreased the level of TGF- $\beta$  in lung metastases and colon tumor, while Cap increased TGF- $\beta$ . Surprisingly, the combination significantly reduced the increase in TGF- $\beta$  induced by Cap (Fig. 7F and G).

Moreover, the intestinal inflammatory environment has a strong influence on the development of intestinal tumor. IL-6 and TNF- $\alpha$  can be rapidly produced during tumorigenesis and the acute inflammatory response [30]. The results showed that DHA reduced the levels of IL-6 and TNF- $\alpha$  in lung metastases and intestinal tumors. More importantly, the combination significantly suppressed IL-6 induced by Cap (Fig. 7H and I). Taken together, DHA could reduce the Cap-induced increase in inflammation.

## 4. Discussion

The commonly used clinical drugs for CRC include 5-Fu, Cap, oxaliplatin, bevacizumab, etc. 5-Fu-based chemotherapy regimens are the standard treatment for adjuvant and advanced CRC, yet about 80 % of patients develop drug resistance [31]. The therapeutic efficacy of 5-Fu is limited by the high toxicity to normal cells and side effects at conventional doses. Further, Cap has been developed as a prodrug of 5-Fu, which improves tumor targeting but is associated with a high incidence of gastrointestinal adverse effects. Oxaliplatin is the third-generation of platinum anticancer drug but often causes severe neurotoxicity, either alone or in combination [32,33]. Even Cap-based combination strategies, such as CapeOx, still cause gastrointestinal toxicity, leading to dose limitation [26]. Therefore, there is an urgent need to find an effective, low-toxicity drug and a new treatment strategy for the clinical treatment of CRC.

Recently, a study showed that DHA inhibited CRC cell proliferation and cell cycle progression by targeting the CDK1/CCNB1/PLK1 signalling pathway [10]. Another study reported that DHA treatment increased c-Myc protein degradation, leading to better inhibition in late-stage CRC [34]. Here, we found that DHA showed a comprehensive inhibitory effect on CRC growth, metastasis and angiogenesis through four animal models. We are more concerned about the improvement of immunosuppression in CRC by DHA. Besides, we compared the inhibition rate of DHA and Cap and found that DHA achieved almost the same inhibitory effect as Cap. It is worth noting that the positive drug Cap showed certain adverse reactions. In the PDX model, mice in Cap group developed severe diarrhoea, and 2 mice in HJG224 suffered intense

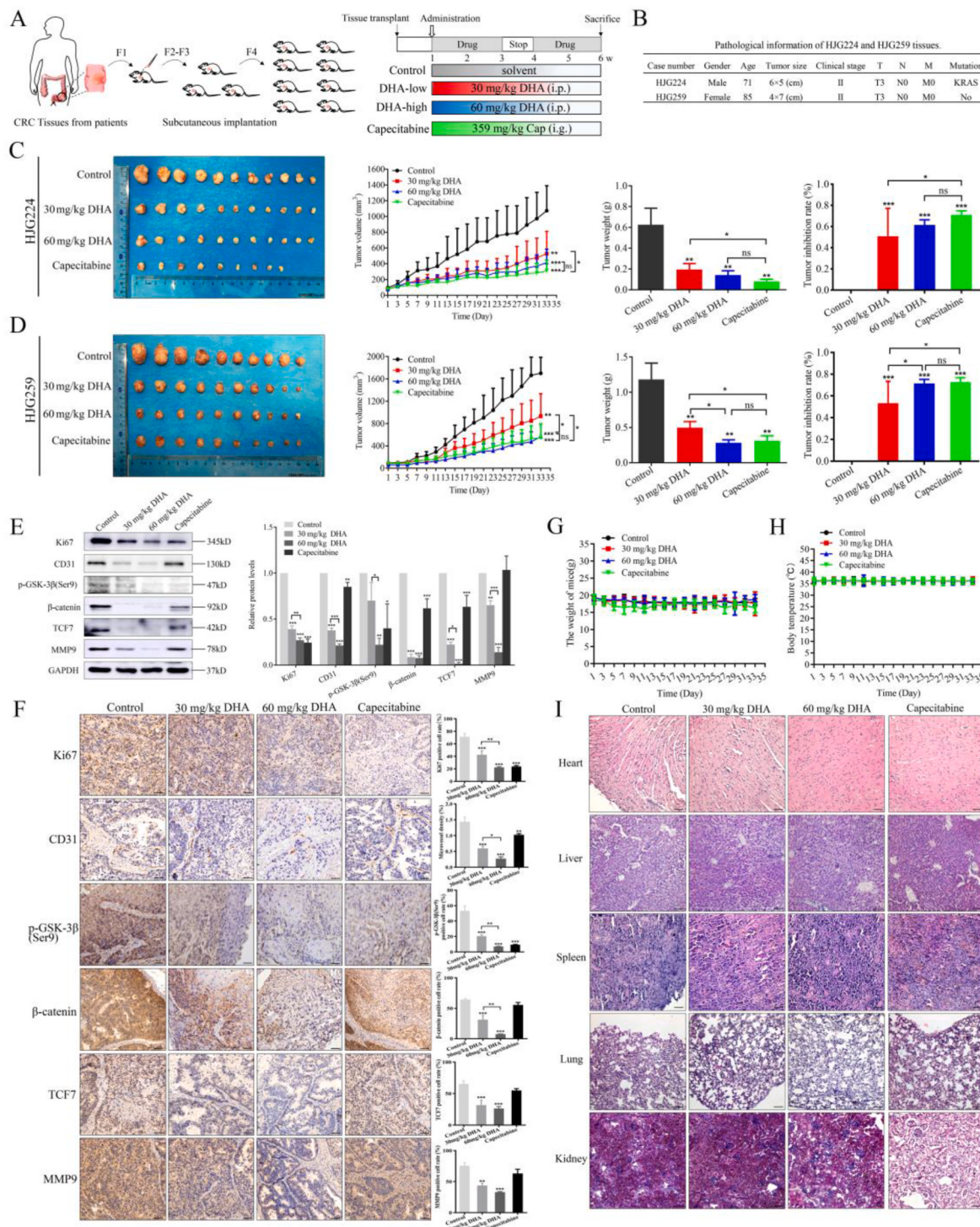


**Fig. 4. DHA inhibits the growth of CRC by GSK-3 $\beta$ /TCF7/MMP9 signaling pathway.** (A) Schematic diagram of the PDX model. (B) The pathological information of HJG224 and HJG259 tissue-derived patients. (C–D) The tumor volume, tumor weight and tumor inhibition rate in HJG224 ( $n = 11$ ) and HJG259 PDX model ( $n = 10$ ). (E–F) The expression levels of Ki67, CD31, p-GSK-3 $\beta$  (Ser9),  $\beta$ -catenin, TCF7, MMP9 in tumor of PDX model (HJG224) were detected by western blotting and IHC. (G–H) The body weight and temperature of mice in PDX model (HJG224). (I) HE staining of heart, liver, spleen, lung and kidney of mice in PDX model (HJG224). The results were shown as the mean  $\pm$  S.D. of three independent experiments. Scale bar = 50  $\mu$ m. (\* $P < 0.05$ , \*\* $P < 0.01$ , \*\*\* $P < 0.001$ ).

weight loss and died. In the CT26 lung metastasis model, nearly half of the mice developed diarrhoea even after only 2 weeks of administration of Cap. Not to mention that in the AOM/DSS model, the weight of the mice fluctuated wildly during the three months of treatment due to severe diarrhoea accompanied by inflammatory intestinal bleeding. These phenomena are consistent with the high incidence of diarrhoea after Cap administration clinically [4]. Conversely, DHA showed no apparent side

effects, regardless of whether it was administered in the short or long term. In the clinical treatment of malaria with DHA, only a few patients suffered from transient reticulocyte reduction. More importantly, the incidence of diarrhoea was significantly reduced by the combination treatment, suggesting that DHA alleviated the adverse effects caused by Cap. Furthermore, the combination of DHA and Cap showed enhanced efficacy and reduced side effects. In addition, the KRAS mutation was

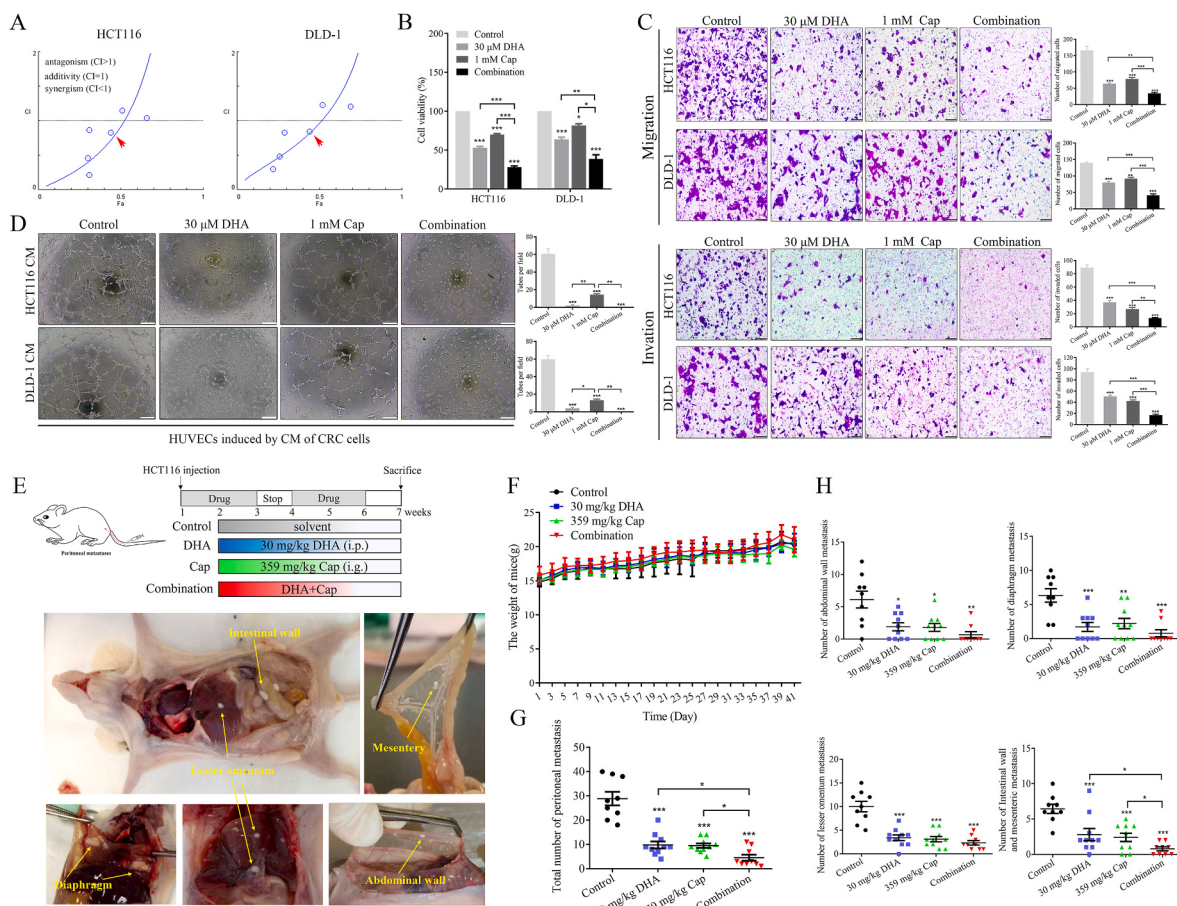


**Fig. 5. The combination of DHA and Cap synergistically inhibits the development of CRC.** (A) The combination index of each combination on CRC cells (the red arrow indicated the final selected concentration: 1 mM Cap and 30  $\mu$ M DHA). (B) The proliferation assay detected the cell viability of CRC cells treated with the combination for 48 h. (C) The migration and invasion ability of CRC cells treated with the combination for 24 h (Scale bar = 100  $\mu$ m) (D) The tube formation of CM-induced HUVECs treated with the combination for 24 h (Scale bar = 200  $\mu$ m) (E) Schematic diagram and anatomic view of peritoneal metastasis. (F) The body weight of mice in peritoneal metastasis model. (G) The total number of peritoneal metastases. (H) The number of metastases in the abdominal wall, lesser omentum, diaphragm, intestinal wall and mesentery. The results were shown as the mean  $\pm$  S.D. of three independent experiments. (\* $P$  < 0.05, \*\* $P$  < 0.01, \*\*\* $P$  < 0.001).

present in both HJG224 tissue-derived patients and CT26 cells that we used in this study. As a common mutation type in CRC with an incidence of about 45 %, KRAS mutation often leads to reduced efficacy of drugs [35]. The significant therapeutic effect of DHA may suggest that DHA is also effective in patients with KRAS mutation.

Herein, DHA directly targeted GSK-3 $\beta$  and promoted the degradation of  $\beta$ -catenin. Moreover, we identified for the first time that p-GSK-3 $\beta$  (Ser9) may be a risk factor in CRC. Moreover, MMP9 is positively correlated with poor prognosis in CRC [36]. In our study, MMP9 was identified as the key molecule in DHA inhibition of CRC development. Furthermore, MMP9 was proved to bind to  $\beta$ -catenin in T cells [37], and downregulation of TCF7 resulted in reduced MMP9 in ovarian cancer cells [38]. However, how TCF7 regulates MMP9 is still unknown. We found for the first time that TCF7 bound to the promoter region of MMP9 in the region of -1000 bp to -500 bp in CRC cells. This finding emphasized the crucial role of the GSK-3 $\beta$ /TCF7/MMP9 pathway during the inhibition of CRC development by DHA. In addition, the combination of DHA and Cap showed the strongest inhibition of p-GSK-3 $\beta$  (Ser9) and MMP9 expression levels (Fig. 6I), which may also explain the synergistic effect of this combination.

Clinically, tumor patients are often accompanied by immunosuppression. Meanwhile, the toxicity and side effects of chemotherapy often weaken their immunity, which may promote tumor recurrence and metastasis. In this study, spleen enlargement was observed in animal models treated with DHA, which raised our concern about the effect of

DHA on immunity. In fact, the potential therapeutic effect of DHA in systemic lupus erythematosus suggests that DHA may restore the Treg/Th17 balance [39]. The spleen is the largest immune organ in the body and contains a large number of lymphocytes, including CD8 $^{+}$ CD3 $^{+}$ T cells. Recent studies have shown that patients with less than 2.2 % CD8 $^{+}$ CD3 $^{+}$ T cells have a four times higher risk of disease progression after surgery [40]. Thus, DHA may help to inhibit the progression of CRC. Additionally, Cap showed immunosuppressive effects, especially with long-term administration. Actually, it has been reported that Cap is an immunosuppressive agent that induces T-cell apoptosis [41]. As known, the immune-excluded-type of tumor is not sensitive to immunotherapy due to the immunosuppressive environment. Mechanistically, the abnormal activation of Wnt/ $\beta$ -catenin signaling is associated with the T-cell exclusion phenotype, which is a major obstacle to many immunotherapies [42]. Interestingly, it has been reported that  $\beta$ -catenin inhibition converts the colorectal tumor microenvironment to an inflammatory T-cell phenotype and enhances the efficacy of the immunotherapy strategy [43]. The effect of DHA on immune function reminds us that the combination of DHA and immunotherapy may help to enhance the anti-cancer effect in the future.

Cancer-related inflammation is known as the seventh hallmark of malignancy [44]. In contrast to sporadic CRC, CAC represents a unique tumorigenesis pathway. Although CAC accounts for only 2 % of CRC cases, inflammation is present at all stages of CRC progression [35]. Indeed, large-scale epidemiological studies have shown that the

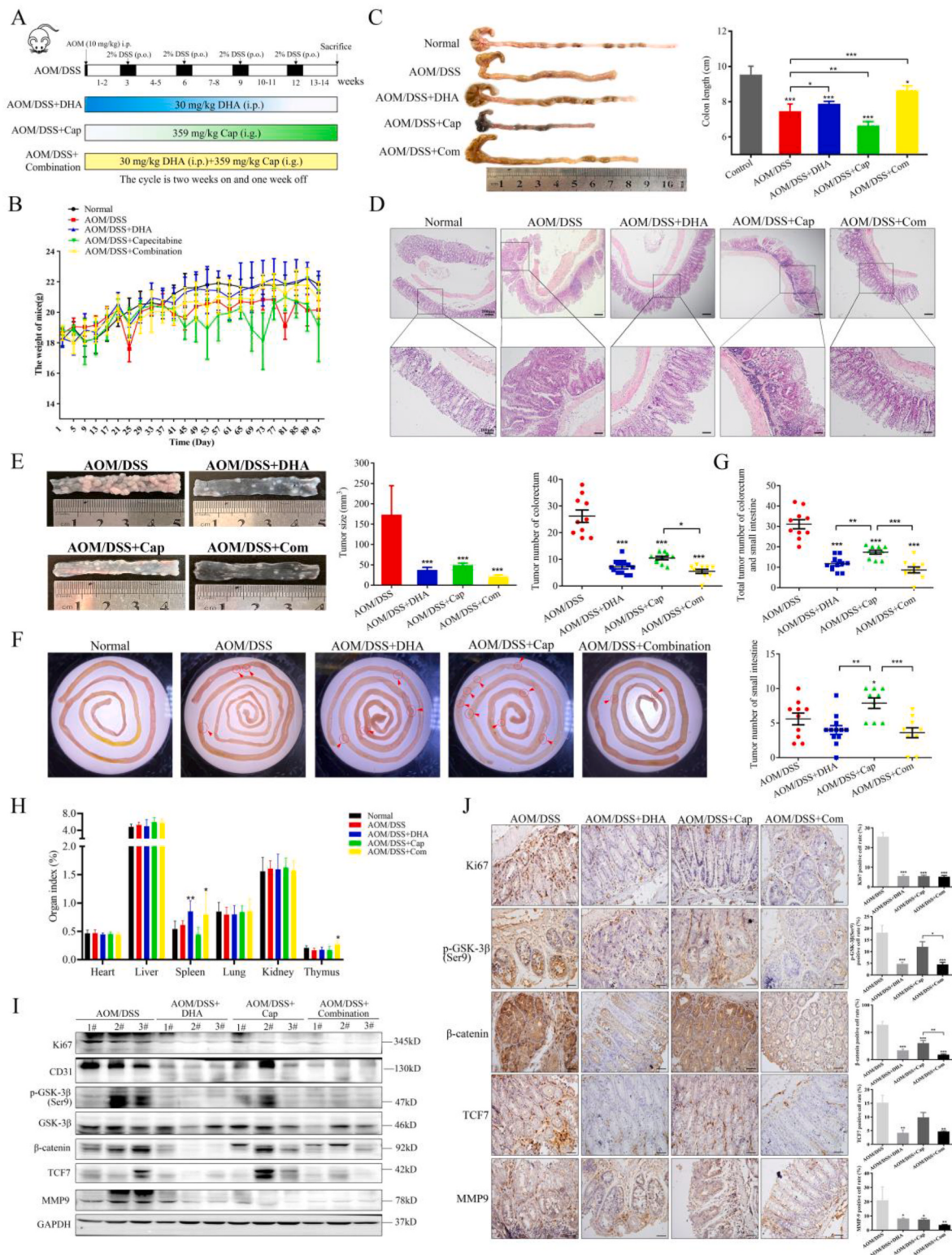


**Fig. 6. The combination of DHA and Cap inhibits colitis-associated CRC.** (A) The schematic diagram of the AOM/DSS model. (B) The body weight of mice during the experiment. (C) Representative images of colorectum in mice and the length statistics. (D) HE staining of the colorectum. (E) Representative images and statistical analysis of colorectal tumor. (F) Representative images and statistical analysis of tumor in small intestine. (G) The total tumor number of colorectum and small intestine. (H) The organ indexes of mice in AOM/DSS model. (I–J) The expressions of Ki67, CD31, p-GSK-3 $\beta$  (Ser9),  $\beta$ -catenin, TCF7 and MMP9 in tumor were detected by western blotting and IHC. The results were shown as the mean  $\pm$  S.D. of three independent experiments. (Scale bar = 50  $\mu$ m) (\* $P$  < 0.05, \*\* $P$  < 0.01, \*\*\* $P$  < 0.001).

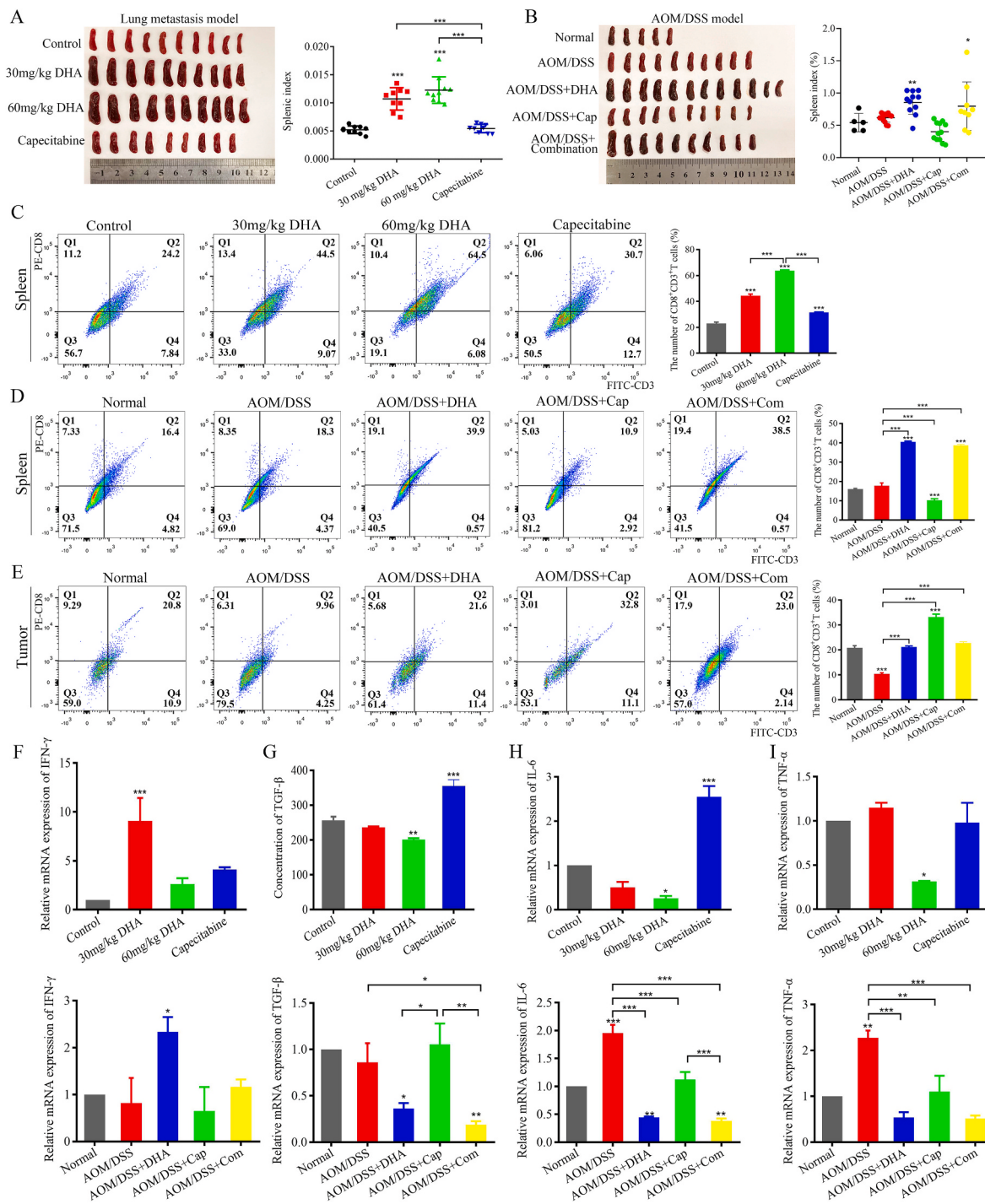


**Fig. 7. The combination alleviates the immunosuppression and inflammation caused by Cap.** (A–B) Spleen volume and index statistics in CT26 lung metastasis model and AOM/DSS model. (C–D) Lymphocytes were extracted from spleen to detect the level of CD8<sup>+</sup>CD3<sup>+</sup>T cells in CT26 lung metastasis model and AOM/DSS model. (E) Lymphocytes were extracted from tumor to detect the level of CD8<sup>+</sup>CD3<sup>+</sup>T cells in AOM/DSS model. (F–I) Relative mRNA expression levels of IFN- $\gamma$ , TGF- $\beta$ , IL-6 and TNF- $\alpha$  of tumor tissues in CT26 lung metastasis model and AOM/DSS model. The results were shown as the mean  $\pm$  S.D. of three independent experiments. (\*P < 0.05, \*\*P < 0.01, \*\*\*P < 0.001).

incidence of CRC is substantially lower in individuals who take nonsteroidal anti-inflammatory drugs, including aspirin [45]. Besides, Bai et al. revealed that DHA inhibited inflammatory responses in the early stage of the AOM/DSS model and subsequent tumor formation [46]. In our study, we compared the role of DHA and Cap in AOM/DSS model and found that the combination of DHA and Cap showed a better inhibitory effect on CAC with good safety and reduced side effects caused by Cap. Clinically, Cap has been reported to induce a

pro-inflammatory response, such as in hand-foot syndrome and dermatomyositis [47]. Notably, Cap significantly increased the number of small intestine tumors compared to the control group. Actually, the incidence of small intestinal tumor is extremely low due to rapid emptying, high concentrations of protective acids and IgA, which could reduce the exposure time between carcinogens and the small intestine [48]. However, if patients have a poor digestive tract, carcinogens may remain in the small intestine and disrupt the intestinal mucosal barrier

[49]. Based on this, we hypothesized that persistent diarrhoea and immunosuppression induced by Cap severely damaged the intestinal barrier and led to an increased number of intestinal tumor. The pro-inflammatory effect induced by Cap suggests that Cap may not be suitable for the treatment of CAC. In contrast, DHA may be a good choice. Remarkably, the combination greatly alleviated the Cap-induced inflammatory response and reduced the side effects, suggesting that it may be an effective strategy for inhibiting CAC and CRC.

Given the results discussed above, we systematically explored the effects and mechanism of DHA in the development of CRC, and evaluated a novel combination for CRC treatment. DHA markedly inhibited the growth, metastasis and angiogenesis of CRC *in vivo* and *in vitro*. Mechanistically, DHA directly targeted GSK-3 $\beta$  and inhibited the GSK-3 $\beta$ /TCF7/MMP9 pathway. Moreover, p-GSK-3 $\beta$  (Ser9) was proven to be a potential biomarker for CRC progression. Importantly, the combination of DHA and Cap showed a better inhibitory effect on CRC and CAC. Meaningfully, this combination enhanced the anti-cancer effect, which was accompanied by the improved immunity, reduced side effect and decreased intestinal tumor number. Nevertheless, our study still has some limitations. Firstly, how DHA inhibits the expression levels of p-GSK-3 $\beta$  (Ser9) and TCF7 needs to be further investigated. Secondly, the design of the treatment plan is complex due to the heterogeneity of the patient population. Here, we only used Cap as the positive control, while the individualized drug administration is lacking. Thus, more clinical drugs are needed as controls to fully evaluate the efficacy of DHA in the future. Thirdly, there are limited clinical trials of DHA in cancer treatment. One study has shown that artemisinin-R (DHA succinate) can improve clinical symptoms in patients with advanced cervical cancer and is well tolerated [50]. Besides, a Phase II clinical trial is investigating the anti-tumor effect of the combination of DHA and icotinib in patients with EGFR-positive NSCLC (NCT03402464). Another is in polycystic ovary syndrome in Phase IV (NCT05465135). Therefore, the clinical efficacy and safety of DHA in CRC need to be validated by further clinical trials. Taken together, this study systematically elucidates the potential of DHA as a low-toxicity and high-efficiency clinical drug for CRC. Furthermore, the combination of DHA and Cap may be a new therapeutic strategy with improved efficacy and reduced side effects.

#### CRediT authorship contribution statement

**Xiaoshuo Dai:** Writing – original draft, Methodology, Data curation, Formal analysis. **Wei Chen:** Writing – original draft, Investigation, Formal analysis. **Yan Qiao:** Resources, Methodology. **Xinhuan Chen:** Resources, Methodology. **Yihuan Chen:** Methodology, Formal analysis. **Kai Zhang:** Methodology, Investigation. **Qiushuang Zhang:** Resources, Methodology. **Xiaoxuan Duan:** Methodology. **Xiang Li:** Resources, Methodology. **Jimin Zhao:** Resources, Methodology. **Fang Tian:** Resources, Methodology. **Kangdong Liu:** Investigation, Formal analysis. **Ziming Dong:** Writing – review & editing, Investigation. **Jing Lu:** Writing – review & editing, Supervision, Funding acquisition, Conceptualization.

#### Declaration of competing interest

The authors declare that they have no known competing financial interests or personal relationships that could have appeared to influence the work reported in this paper.

#### Acknowledgements

This work was supported by the National Natural Science Foundation of China (81572972), the Supporting Plan of Scientific and Technological Innovation Team in Universities of Henan Province (20IRTSTHN029) and the Key Research Program of Higher Education Institutions in Henan Province (24A310020).

#### Appendix A. Supplementary data

Supplementary data to this article can be found online at <https://doi.org/10.1016/j.canlet.2023.216596>.

#### Abbreviations

AOM	azoxymethane
CAC	colitis-associated cancer
Cap	capecitabine
ChIP	chromatin immunoprecipitation
CM	conditioned medium
Co-IP	coimmunoprecipitation
CRC	colorectal cancer
DHA	dihydroartemisinin
DSS	dextran sodium sulfate
ECM	endothelial cell medium
GSK-3 $\beta$	glycogen synthase kinase-3 $\beta$
HE	haematoxylin and eosin
HUVECs	human umbilical vein endothelial cells
IBD	inflammatory bowel disease
IHC	immunohistochemical staining
MD	molecular dynamics
PDX	patient-derived xenografts
RMSD	root mean square deviation

#### References

- [1] H. Sung, et al., Global cancer statistics 2020: GLOBOCAN estimates of incidence and mortality worldwide for 36 cancers in 185 countries, CA Cancer J Clin 71 (3) (2021) 209–249.
- [2] M. Arnold, et al., Global patterns and trends in colorectal cancer incidence and mortality, Gut 66 (4) (2017) 683–691.
- [3] E. Dekker, P.J. Tanis, J.L.A. Vleugels, P.M. Kasi, M.B. Wallace, Colorectal cancer, Lancet 394 (10207) (2019) 1467–1480.
- [4] M.B. Visacri, et al., Adverse reactions and adherence to capecitabine: a prospective study in patients with gastrointestinal cancer, J. Oncol. Pharm. Pract. 28 (2) (2022) 326–336.
- [5] Chinese Society of Gastroenterology, C.C.G.o.C.S.o.G.C.M.A, Chinese consensus on prevention of colorectal neoplasia (2021, Shanghai), J. Dig. Dis. 23 (2) (2022) 58–90.
- [6] T. Hoang, D.K. Sohn, B.C. Kim, Y. Cha, J. Kim, Efficacy and safety of systemic treatments among colorectal cancer patients: a network meta-analysis of randomized controlled trials, Front. Oncol. 11 (2021) 756214.
- [7] Y.Y. Tu, The discovery of artemisinin (qinghaosu) and gifts from Chinese medicine, Nat. Med. 17 (10) (2011) 1217–1220.
- [8] X. Dai, et al., Dihydroartemisinin: a potential natural anticancer drug, Int. J. Biol. Sci. 17 (2) (2021) 603–622.
- [9] Y. Yu, et al., Dihydroartemisinin enhances the anti-tumor activity of oxaliplatin in colorectal cancer cells by altering PRDX2-reactive oxygen species-mediated multiple signaling pathways, Phytomedicine 98 (2022) 153932.
- [10] Y.C. Yi, et al., Dihydroartemisinin suppresses the tumorigenesis and cycle progression of colorectal cancer by targeting CDK1/CCNB1/PLK1 signaling, Front. Oncol. 11 (2021) 768879.
- [11] H. Zhao, et al., Wnt signaling in colorectal cancer: pathogenic role and therapeutic target, Mol. Cancer 21 (1) (2022) 144.
- [12] A.S. Aghabozorgi, et al., The genetic factors associated with Wnt signaling pathway in colorectal cancer, Life Sci. 256 (2020) 118006.
- [13] M. Leost, et al., Paullones are potent inhibitors of glycogen synthase kinase-3beta and cyclin-dependent kinase 5/p25, Eur. J. Biochem. 267 (19) (2000) 5983–5994.
- [14] A. Martinez, C. Gil, D.I. Perez, Glycogen synthase kinase 3 inhibitors in the next horizon for Alzheimer's disease treatment, Int. J. Alzheimer's Dis. 2011 (2011) 280502.
- [15] M. Bauer, M. Adli, R. Ricken, E. Severus, M. Pilhatsch, Role of lithium augmentation in the management of major depressive disorder, CNS Drugs 28 (4) (2014) 331–342.
- [16] G. Jin, et al., Combination curcumin and (-)-epigallocatechin-3-gallate inhibits colorectal carcinoma microenvironment-induced angiogenesis by JAK/STAT3/IL-8 pathway, Oncogenesis 6 (10) (2017) e384.
- [17] J.L. Stamos, M.L. Chu, M.D. Enos, N. Shah, W.I. Weis, Structural basis of GSK-3 inhibition by N-terminal phosphorylation and by the Wnt receptor LRP6, Elife 3 (2014) e01998.
- [18] G.M. Morris, et al., AutoDock4 and AutoDockTools4: automated docking with selective receptor flexibility, J. Comput. Chem. 30 (16) (2009) 2785–2791.
- [19] T. Iwai, et al., Continuous administration of bevacizumab plus capecitabine, even after acquired resistance to bevacizumab, restored anti-angiogenic and antitumor

- effect in a human colorectal cancer xenograft model, *Oncol. Rep.* 36 (2) (2016) 626–632.
- [20] S.M. Parizadeh, et al., Targeting cancer stem cells as therapeutic approach in the treatment of colorectal cancer, *Int. J. Biochem. Cell Biol.* 110 (2019) 75–83.
- [21] Y. Ai, et al., Pull the plug: anti-angiogenesis potential of natural products in gastrointestinal cancer therapy, *Phytother. Res.* (2022) 3371–3393.
- [22] Y. Sato, et al., Signal transduction and transcriptional regulation of angiogenesis, *Adv. Exp. Med. Biol.* 476 (2000) 109–115.
- [23] K. Takahashi, Y. Sawasaki, J. Hata, K. Mukai, T. Goto, Spontaneous transformation and immortalization of human endothelial cells, *In Vitro Cell. Dev. Biol.* 26 (3 Pt 1) (1990) 265–274.
- [24] Q. Zhang, et al., Improved antitumor efficacy of combined vaccine based on the induced HUVECs and DC-CT26 against colorectal carcinoma, *Cells* 8 (5) (2019) 494.
- [25] E. Izumchenko, et al., Patient-derived xenografts effectively capture responses to oncology therapy in a heterogeneous cohort of patients with solid tumors, *Ann. Oncol.* 28 (10) (2017) 2595–2605.
- [26] A.V. Kalidindi, B. Dubashi, M. Jayanthi, D.G. Shewade, Efficacy and safety of capecitabine and oxaliplatin (CAPOX) treatment in colorectal cancer: an observational study from a tertiary cancer center in South India, *Indian J. Cancer* 59 (1) (2022) 73–79.
- [27] M. Jakovljevic, Global, regional, and national burden of colorectal cancer and its risk factors, 1990–2019: a systematic analysis for the Global Burden of Disease Study 2019 (vol 7, pg 627, 2022), *Lancet Gastroenterol. Hepatol.* 7 (8) (2022) 627–647.
- [28] S. Shalapour, M. Karin, Cruel to Be kind: epithelial, microbial, and immune cell interactions in gastrointestinal cancers, *Annu. Rev. Immunol.* 38 (2020) 649–671.
- [29] M. Reina-Campos, N.E. Schärping, A.W. Goldrath, CD8(+) T cell metabolism in infection and cancer, *Nat. Rev. Immunol.* 21 (11) (2021) 718–738.
- [30] A. Pawlowska-Kamienska, P. Krawiec, E. Pac-Kozuchowska, Interleukin 6: biological significance and role in inflammatory bowel diseases, *Adv. Clin. Exp. Med.* 30 (4) (2021) 465–469.
- [31] D.B. Longley, W.L. Allen, P.G. Johnston, Drug resistance, predictive markers and pharmacogenomics in colorectal cancer, *Biochim. Biophys. Acta* 1766 (2) (2006) 184–196.
- [32] T. Aoyama, et al., Effects of Goshajinkigan (TJ-107) for oxaliplatin-induced peripheral neurotoxicity using the functional assessment of cancer therapy/gynecologic oncology group 12-item neurotoxicity questionnaire in a Phase II, multicenter, randomized, double-blind, placebo-controlled trial, *J. Cancer Res. Therapeut.* 17 (6) (2021) 1473–1478.
- [33] P. de Albuquerque Ribeiro Gondimho, et al., FLOX (5-fluorouracil + leucovorin + oxaliplatin) chemotherapy for colorectal cancer leads to long-term orofacial neurotoxicity: a STROBE-guided longitudinal prospective study, *Int. J. Clin. Oncol.* 25 (12) (2020) 2066–2074.
- [34] X.J. Hu, et al., Dihydroartemisinin is potential therapeutics for treating late-stage CRC by targeting the elevated c-Myc level, *Cell. Death Dis.* 12 (11) (2021) 1053.
- [35] J. Li, X. Ma, D. Chakravarti, S. Shalapour, R.A. DePinho, Genetic and biological hallmarks of colorectal cancer, *Genes Dev.* 35 (11–12) (2021) 787–820.
- [36] R. Peltonen, et al., High expression of MMP-9 in primary tumors and high preoperative MPO in serum predict improved prognosis in colorectal cancer with operable liver metastases, *Oncology* 99 (3) (2021) 144–160.
- [37] B. Wu, S.P. Crampton, C.C. Hughes, Wnt signaling induces matrix metalloproteinase expression and regulates T cell transmigration, *Immunity* 26 (2) (2007) 227–239.
- [38] Z. Bai, et al., Downregulation of GPR4 and TCF7 promotes apoptosis and inhibits growth and invasion of ovarian cancer cells, *Anti Cancer Agents Med. Chem.* 21 (12) (2021) 1544–1550.
- [39] Y. Chen, T. Tao, W. Wang, B. Yang, X. Cha, Dihydroartemisinin attenuated the symptoms of mice model of systemic lupus erythematosus by restoring the Treg/Th17 balance, *Clin. Exp. Pharmacol. Physiol.* 48 (4) (2021) 626–633.
- [40] C.S. Jansen, et al., An intra-tumoral niche maintains and differentiates stem-like CD8 T cells, *Nature* 576 (7787) (2019) 465–470.
- [41] S. Zhang, et al., Capecitabine can induce T cell apoptosis: a potential immunosuppressive agent with anti-cancer effect, *Front. Immunol.* 12 (2021) 737849.
- [42] P.S. Hegde, D.S. Chen, Top 10 challenges in cancer immunotherapy, *Immunity* 52 (1) (2020) 17–35.
- [43] C. Wang, et al., beta-Catenin inhibition shapes tumor immunity and synergizes with immunotherapy in colorectal cancer, *OncolImmunology* 9 (1) (2020) 1809947.
- [44] F. Colotta, P. Allavena, A. Sica, C. Garlanda, A. Mantovani, Cancer-related inflammation, the seventh hallmark of cancer: links to genetic instability, *Carcinogenesis* 30 (7) (2009) 1073–1081.
- [45] X.W. Hua, et al., Timing of aspirin and other nonsteroidal anti-inflammatory drug use among patients with colorectal cancer in relation to tumor markers and survival, *J. Clin. Oncol.* 35 (24) (2017) 2806–2813.
- [46] B.J. Bai, et al., Therapeutic effects of dihydroartemisinin in multiple stages of colitis-associated colorectal cancer, *Theranostics* 11 (13) (2021) 6225–6239.
- [47] X. Liao, et al., SNPs in the COX-2/PGES/EP signaling pathway are associated with risk of severe capecitabine-induced hand-foot syndrome, *Cancer Chemother. Pharmacol.* 85 (4) (2020) 785–792.
- [48] S. Melgar, A. Bas, S. Hammarstrom, M.L. Hammarstrom, Human small intestinal mucosa harbours a small population of cytolytically active CD8+ alphabeta T lymphocytes, *Immunology* 106 (4) (2002) 476–485.
- [49] A. Vanoli, et al., Small bowel carcinomas in celiac or Crohn's disease: distinctive histopathologic, molecular and histogenetic patterns, *Mod. Pathol.* 30 (10) (2017) 1453–1466.
- [50] F.H. Jansen, et al., First study of oral Artenimol-R in advanced cervical cancer: clinical benefit, tolerability and tumor markers, *Anticancer Res.* 31 (12) (2011) 4417–4422.